Eur. Phys. J. A (2025) 61:190
https://doi.org/10.1140/epja/s10050-025-01655-w

THE EUROPEAN PHYSICAL JOURNAL A

Regular Article - Experimental Physics

Fission product mass distribution studies in ^{35}Cl + ^{176}Yb and ^{35}Cl + ^{165}Ho reactions

S. Kumar[1,a], **R. Tripathi**[1,3], **S. Patra**[1,3], **A. Mhatre**[1], **A. Kumar**[1], **K. Ramachandran**[2], **T. N. Nag**[1], **S. Santra**[2,3]

[1] Radiochemistry Division, Bhabha Atomic Research Centre, Mumbai 400085, India
[2] Nuclear Physics Division, Bhabha Atomic Research Centre, Mumbai 400085, India
[3] Homi Bhabha National Institute, Anushaktinagar, Mumbai 400094, India

Received: 13 March 2025 / Accepted: 30 July 2025

Communicated by Silvia Leoni.

Abstract Many studies on the fission fragment mass distribution in the sub-lead and pre-actinide region have proposed the presence of asymmetric components in this mass region, primarily due to proton shells corresponding to Z ≈ 36, 38. Present studies have been carried out to investigate the mass distributions in the ^{35}Cl + ^{176}Yb → ^{211}Fr and ^{35}Cl + ^{165}Ho → ^{200}Po reactions in the mass region around ~ 200, a transition between the sub-lead and actinide region. Mass distribution studies have been carried out near the entrance channel Coulomb barrier using the recoil catcher technique, followed by off-line γ-ray spectrometry of the fission products. The broad Gaussian nature of the mass distribution in the ^{35}Cl + ^{176}Yb reaction indicates a dominant symmetric fission contribution. The mass distributions for the ^{35}Cl + ^{176}Yb and ^{35}Cl + ^{165}Ho reactions were found to be in gross agreement with GEF (Schmidt et al. in Nucl Data Sheets 131:107, 2016; Schmidt and Jurado in Rep Prog Phys 81:106301, 2018). The GEF model predicts a dominant symmetric fission contribution along with the contribution from the asymmetric fission mode corresponding to $Z \approx 38$. The most probable charge, Z_P was varied within a range of ± 1.5 units with respect to that obtained using the unchanged charge density hypothesis to obtain the best agreement with GEF. However, a few experimental mass yields in the mass regions corresponding to Z ≈ 50–52 and $Z \approx 54$–56 were observed to be still higher (more than ~ 50%) compared to the GEF predictions. A similar enhancement observed in the corresponding fission product yields indicates possible contributions from the conventional asymmetric fission modes, in addition to the shell corresponding to Z ≈ 38.

1 Introduction

The fission product mass distribution is intimately connected to the potential energy landscape of the fissioning nucleus. Subsequent to the observation of asymmetric mass distribution in the beta delayed fission of ^{180}Tl [3], a large number of studies have been carried out theoretically and experimentally in the pre-actinide as well as sub-lead mass regions [4–30]. The experimentally observed asymmetric mass distributions in the pre-actinide region have been explained based on the states of the fissioning nucleus in the vicinity of the saddle point [4–6] as well as of pre-formed fragments near the scission point [7–12]. In the first approach, shell gaps arising due to the interaction of [30 Λ Ω] and [41 Λ Ω] levels of the fissioning nucleus have been proposed to be the driving force for the contribution from asymmetric fission [4]. On the other hand, Wilkins et al. proposed fragment shell effects near the scission point to be the dominant factor responsible for the asymmetric fission in very early studies [7]. Recently, different neutron and proton shells have been proposed in the octupole deformed fragments near scission [11, 12]. Studies in the mass region around A ≈ 200 are crucial for observing the transition from asymmetric fission in the sub-lead region to that in the actinide region, via the intermediate pre-actinide mass range. It might be possible to observe the role of the neutron/proton shells operating in the sub-lead as well as in the actinide region in the mass distribution of the fissioning nuclei around A ≈ 200. The low-energy fission studies carried out by Schmidt et al. [13] over a wide range of nuclei from ^{205}At to ^{234}U showed dominant symmetric charge distributions for lower mass fissioning systems around the lead region. In contrast, significant contribution from asymmetric fission was observed in the higher mass region, showing a transition around ^{227}Th. There have been a large number of

[a] e-mail: ksatyam@barc.gov.in (corresponding author)

Published online: 14 August 2025

studies in the recent past as well as some early studies spanning over a wide mass range around A ≈ 176–210 [15–30]. Recently, detailed fission fragment mass distribution studies have been carried out by Bogachev et al. [27] and Kozulin et al. [28] covering fissioning systems ^{178}Pt, ^{180,182,182,190}Hg and ^{184,192,202}Pb. Based on these studies, it has been proposed that the asymmetric components in the multi-modal fission in this mass region mainly arises due to the proton shells corresponding to Z ≈ 36 and 38 (referred to as A1 mode), 45 and 46 (referred to as A2 mode) and 28/50 (referred to as A3 mode) [27, 28]. The proton shell corresponding to Z ≈ 50, as observed in these studies, can also be related to the conventional SI asymmetric mode [31]. In the study of fission fragment mass distributions carried out by Itkis et al. [15], contributions from conventional SI and SII modes were observed in the fission fragment mass distributions in the light fissioning systems ^{205,207,209}Bi, ^{208,210,212}Po and ^{213}At. In all these systems, mass distributions were observed to have a flat-top nature near symmetry, which is now attributed to the proton shell closure (Z ≈ 36–38) [15, 30].[1]Morfouace et al. [32] studied the charge distributions of fission fragments for 100 exotic fissioning systems ranging from the sub-lead to the actinide region. The study demonstrated a transition to more asymmetric fission as we move towards neutron-deficient systems. The study highlighted the dominant role of deformed proton shell at Z = 36 of the light fragment in the fission of sub-lead nuclei [32]. The fission fragment mass distributions studies for ^{176,186}Pt at varying excitation energies by [2]Duan et al. [33] inferred the role of the proton shells corresponding to $Z \approx 35$ for the light fragments and $Z \approx 43$ for the heavy fragments. In this study, the presence of asymmetric fission mode was observed at high excitation energies which was attributed to the contribution from higher chance fission with low excitation energies. Similarly, heavy-ion induced fission mass distributions for the even-Z fissioning nuclei ranging from ^{144}Gd to ^{212}Th studied by [3]Buete et al. [34] attributed the proton shell gaps at Z = 34, 36 and Z = 44, 46 to be major guide for the fission mass distributions in the sub-lead region. However, the study didn't rule out the contribution from the proton shells associated with asymmetric modes SI and SII fission [34]. The proton number of fragments can be estimated using the unchanged charge density (UCD) hypothesis, which assumes the same N/Z ratio for fragments and the fissioning nucleus [35]. In a recent study on the fission of ^{178}Hg, it was pointed out that $<N>/Z$ values may significantly deviate from calculations based on the UCD hypothesis due to charge polarization effects. However, the observed deviation for such a light mass fissioning nucleus was in the opposite direction compared to that observed in the actinide region [26]. Change in the direction of the deviation reflects the shift of the Z_P values towards the neutron-deficient region in the light mass fissioning system. Based on these studies, strong roles of Z = 28 and Z = 50 shells were also observed in governing the mass distribution. The study was carried out using inverse kinematics at VAMOS++ where, mass and charge identification of one of the fragments were obtained from time-of-flight (TOF) measurement, while the fission partner was detected by the second detection (SED) arm consisting of a position-sensitive MWPC (PS-MWPC) backed with a Si detector [26]. The information about Z of the fission products (mostly for products with even N and even Z) can also be obtained using γ-γ coincidence measurement of the prompt γ-rays emitted near the end of the yrast decay cascade [36, 37]. Also, the information about the proton number of the fission products can be obtained using radiochemical methods, which involves irradiation followed by off-line γ-ray spectrometry of the radioactive fission products. Off-line γ-ray spectrometry is an alternative or complementary approach to the on-line measurements and has been extensively used in the recent past [38–44]. In this method, the fission product of a given mass and proton number can be uniquely identified by identifying its characteristic decay γ-rays as well as following its half-life.

In the present study, the fission product mass distribution of the ^{35}Cl + ^{176}Yb → ^{211}Fr reaction has been measured using off-line γ-ray spectrometry at E_{lab} = 167.1 MeV. Experimentally measured fission product cross-sections were modified to obtain the corresponding mass yields using the respective charge distribution parameters. Results from the ^{35}Cl + ^{176}Yb → ^{211}Fr reaction have been compared with the results obtained for the ^{35}Cl + ^{165}Ho → ^{200}Po reaction at 161.7 MeV beam energy from a separate experiment, to obtain a comprehensive understanding of the role of different shells in the pre-actinide region. A detailed comparison of the experimental mass yields with those calculated using the GEF code [1, 2] has been carried out for both the fissioning systems.

2 Experimental details

The experiments were carried out at the BARC-TIFR Pelletron-LINAC facility at Tata Institute of Fundamental Research, Mumbai, India. For the ^{35}Cl + ^{176}Yb reaction, a self-supporting ^{176}Yb target (Yb target 96.6% enriched in ^{176}Yb isotope) of thickness ~ 2.2 mg/cm^2 was mounted on a target stand. A Pb foil of thickness ~ 17.5 mg/cm^2 was used as a forward catcher foil to capture the fission products in the forward direction. The energy of the ^{35}Cl beam emerging from the target was much below the fusion barrier for lead, thereby avoiding any possibility of fission products from ^{35}Cl + ^{nat}Pb reaction. For the collection of fission products recoiling out

[1,2,3] The references have been included during the revision of the manuscript.

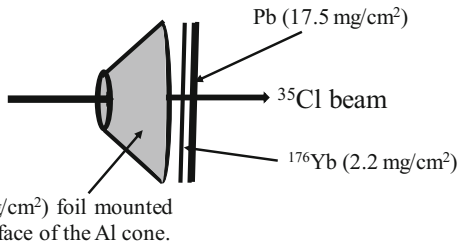

Fig. 1 Schematic diagram of the irradiation setup for the ^{35}Cl + ^{176}Yb reaction

in the backward direction of the beam, an Al foil of thickness 6.75 mg/cm^2 was placed on the inner surface of an aluminium cone as the backward catcher foil. The aluminium cone had a 5 mm diameter hole at the centre to allow the passage of the beam. The ^{176}Yb target was irradiated with a ^{35}Cl beam of energy 167.1 MeV for approximately 63 h. The excitation energy and the E_{CM}/V_C value corresponding to the beam energy were calculated to be 61 MeV and 1.04, respectively, where E_{CM} is the beam energy in the centre of mass frame of reference and V_C is the entrance channel Coulomb barrier. Beam intensity was continuously monitored using flux mapping [45] at every 30 s during irradiation to account for the fluctuations, if any, during the irradiation. The schematic of the experimental setup for the ^{35}Cl + ^{176}Yb reaction is shown in Fig. 1.

The target, along with the catcher foils (forward as well as backward), was mounted on a single perspex plate after irradiation and was subjected to off-line γ-ray spectrometry. Pre-calibrated high-resolution γ-ray spectrometers coupled to a PC based multi-channel analyzer (MCA) were used to acquire the γ-ray spectra of the fission products. Two high-purity coaxial germanium (HPGe) detectors with a relative efficiency of approximately 30% and energy resolution of 1.94 (D1) and 2.01 (D2) keV FWHM at 1332 keV γ-ray energy of ^{60}Co were used for the γ-ray spectrometry. A standard ^{152}Eu^{g} γ-ray source, counted at a distance identical to that in the case of the sample, was used for the energy and the absolute efficiency calibration of the HPGe detectors. The dead time of the HPGe detectors was kept below 1% to avoid the pile-up effect during the counting of the irradiated samples. Several γ-ray spectra of the fission products were acquired covering a range of cooling periods from $\approx$ 10 min to $\approx$ 70 days. The unambiguous identification of the fission products was carried out by matching their characteristic decay γ-ray energy, as well as by following their decay profile to ensure half-life matching. The acquired γ-ray spectra at two different cooling times are shown in Fig. 2.

In a separate experiment, a self-standing ^{165}Ho target of thickness 22 mg/cm^2 was irradiated with a ^{35}Cl beam of energy 165.7 MeV for approximately 36 h. As a different approach, a thick target of ^{165}Ho was used to avoid the undesired background in the γ-ray spectra due to the products arising from the interaction of the beam with the catcher foil. However, there would be significant decrease in the energy of the beam as it traverses through the thick target. The average beam energy in the target, weighted over the fusion cross-section, was obtained as 161.7 MeV. The fusion cross-section was calculated as a function of beam energy using the code CCFUS [46]. The uncertainty in the average beam energy, arising due to the energy loss as it passed through the target, was estimated to be 3.3 MeV. The thickness of the target effectively contributing to fission was obtained to be approximately 1.3 mg/cm^2. Fission products will be preferentially forward-focused due to the large recoil momentum brought in by the heavy beam. The ^{165}Ho target, after irradiation with the ^{35}Cl beam, was subjected to the off-line γ-ray spectrometry as discussed above. The excitation energy and the E_{CM}/V_C value corresponding to the beam energy were calculated to be 56.4 MeV and 1.03, respectively. The uncertainty in the excitation energy was calculated to be 2.7 MeV.

To avoid any possibility of wrong assignment due to γ-ray spectral interferences, yields of only those fission products have been included, which satisfy the conditions regarding matching of the characteristic γ-ray energy as well as expected decay profile based on the half-life. Decay data such as half-lives, γ-ray energies, and their abundances for the fission products identified in the present study are given in Table 1 [47–49]. A total of 47 and 30 fission products were identified using their γ-rays and half-lives for the ^{35}Cl + ^{176}Yb and ^{35}Cl + ^{165}Ho reactions, respectively.

The acquired γ-ray spectra were analyzed using the peak area analysis software PHAST [50] to obtain the peak areas corresponding to the characteristic γ-rays of the fission products. The γ-ray peak areas were used to obtain the 'end of irradiation' activities, A of the fission products at different cooling times using Eq. (1):

$$A = PA \times \left(\frac{CT}{LT}\right) / \left[a_\gamma \cdot \varepsilon_\gamma \cdot [exp\,(-\lambda \cdot T_{cool})] \cdot \left[\frac{(1 - exp\,(-\lambda \cdot CT))}{\lambda}\right]\right] \quad (1)$$

where, *PA* denotes the peak area of the characteristic γ-ray of the fission products, CT and LT are the clock time and live time of the spectra acquisition, respectively, a_γ is the abundance (photons/disintegration) of the corresponding γ-ray, ε_γ is the efficiency of the detector for the corresponding γ-ray, λ is the decay constant of the fission product, and T_{cool} is the cooling time from the end of irradiation till the start of the spectra acquisition. The formation cross-section (σ) of the identified fission products at different cooling times was obtained from the 'end of irradiation' activities using

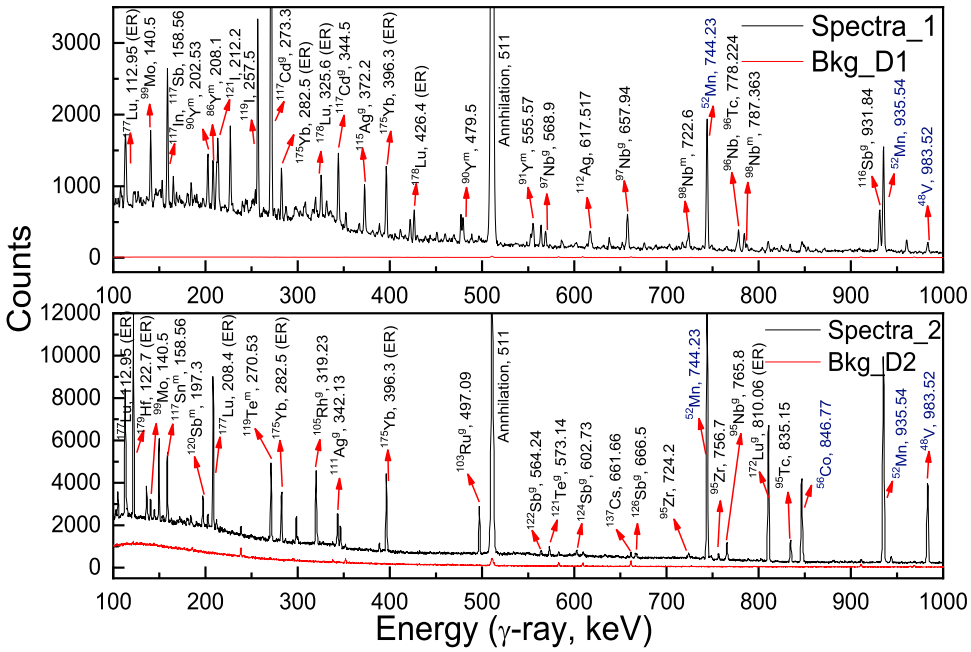

Fig. 2 The acquired γ-ray spectra of the target and the catcher foils at two different cooling times for the ^{35}Cl + ^{176}Yb reaction at 167.1 MeV beam energy. The background in both spectra has been normalized with respect to the acquisition time of the γ-ray spectra. Spectra_1 was acquired for 1000 s after cooling for ~ 82 min, and Spectra_2 was acquired for 100,000 s after cooling for ~ 16 days. Products arising from the reaction of the beam with materials other than the ^{176}Yb target are marked in blue colour. Products marked as ER in the spectra refer to the evaporation residue formed by transfer/pickup reactions. A featureless background spectrum at shorter cooling time is due to the large count rate from the irradiated sample compared to the background count rate

the standard activation equation [45]:

$$\sigma = \frac{A}{N\sum_{k=1}^{M}(1 - exp(-\lambda\Delta t))\phi_k exp(-\lambda(T_{irr} - T_k))} \quad (2)$$

where, N is the number of target atoms per cm^2, λ is the decay constant, T_{irr} is the duration of irradiation, Φ_{k} is the number of beam particles incident per unit time in k^{th} time interval, Δt is the duration of the time interval, T_{k} is the clock time at the end of k^{th} interval and M $(= T_{\mathrm{irr}}/\Delta t)$ is the number of intervals in the irradiation time. Beam intensity was continuously monitored during irradiation to account for the fluctuations, if any, during the irradiation. The beam intensity was measured every 30 s. The average beam intensity was found to be $(2.81 \pm 1.18) \times 10^9$ beam particles/s for the beam energy of 161.7 MeV for the ^{35}Cl + ^{176}Yb reaction. The large standard deviation in the beam current is due to the beam intensity fluctuations as well as breaks during the irradiation, which is taken care of by the flux mapping. The overall formation cross-section of a given fission product has been calculated by error-weighted average of the individual cross-sections at different cooling times. The uncertainty in the measured formation cross-section of the fission product includes the uncertainty associated with the peak area of its characteristic γ-rays. It should be mentioned here that the fission products showing consistency in the formation cross-sections for about 2–3 half-lives have been used for obtaining the mass distribution. In the cases where the parent isotope decays to the daughter isotope, which is in equilibrium with the parent, the individual contribution of parent and daughter in the overall calculated yield of the daughter isotope was obtained using the parent-daughter decay-growth equation. Through this method, the independent cross-section of the daughter isotope and the cumulative/independent (if no precursor contribution) cross-sections of the parent were obtained. In the case of more than one radionuclide decaying through the same γ-ray energy (as in the case of ^{117}In$^{\mathrm{g}}$ and ^{117}Sb, both decaying through 158.56 keV energy), peak areas at different cooling times were fitted using the mixed activity equation to obtain the individual cross-section of the contributing fission products. The formation cross-sections of the fission products identified in the ^{35}Cl + ^{176}Yb reaction at 167.1 MeV are given in Table 2.

Similarly, the γ-ray spectra acquired for the ^{35}Cl + ^{165}Ho reaction at 161.7 MeV were analyzed using the software PHAST [50]. The 'end of irradiation' activity of the fission products at different cooling times identified in the ^{35}Cl + ^{165}Ho reaction was obtained using the peak areas of the corresponding γ-rays, which was further used to obtain the fission product yields. Here, the absolute cross-sections could not be measured due to the loss of fission products in the backward hemisphere and the use of a thick target. For the cases where the yields of a fission product were obtained using more than one γ-ray in the ^{35}Cl + ^{165}Ho reaction, the overall yield of the fission product was obtained using the error-weighted average of the yields. The uncertainty in the measured yields includes the uncertainty associated with the peak area of the characteristic γ-ray.

The sources of uncertainty in the measured yield of the fission products arise mainly due to the uncertainty in the peak areas of the characteristic γ-rays of the fission products and the uncertainty in the efficiency calibration. The

Table 1 The nuclear data used for the fission products identified in the present study [47–49]

$^{35}Cl + ^{176}Yb$				$^{35}Cl + ^{165}Ho$			
Nuclide	Half-life	Eγ (keV)	Abun. (%)	Nuclide	Half-life	Eγ (keV)	Abun. (%)
$^{71}Zn^{m}$	4.137 h	386.37	89.0	$^{69}Zn^{m}$	13.756 h	438.64	94.85
$^{72}Zn \rightarrow {}^{72}Ga$ [b]	46.5 h			^{72}Ga	14.025 h	629.97	26.13
^{72}Ga	14.025 h	629.97	26.13	^{76}As	26.24 h	559.1	45.0
^{73}Ga	4.87 h	297.32	79.8	$^{82}Br^{g}$ [a]	35.284 h	554.35	71.7
^{74}As	17.78 d	595.83	59			619.11	43.7
^{76}As	26.24 h	559.1	45.0			698.36	28.4
^{77}Ge	11.211 h	264.45	53.3			776.5	83.6
$^{82}Br^{g}$	35.284 h	776.5	83.6			1044.01	26.9
$^{84}Rb^{g}$	32.82 d	881.60	68.9			1317.49	27.6
$^{86}Rb^{g}$	18.671 d	1077	8.64	$^{87}Y^{m}$	13.37 h	380.79	78.05
$^{90}Y^{m}$	3.232 h	202.53	97.0	$^{90}Y^{m}$ [a]	3.232 h	202.53	97.0
$^{91}Sr \rightarrow {}^{91}Y^{m}$ [b]	9.68 h					479.51	90.5
$^{91}Y^{m}$	49.7 min	555.57	95	$^{91}Sr \rightarrow {}^{91}Y^{m}$ [b]	9.68 h		
^{92}Sr	2.61 h	1383.93	90	$^{91}Y^{m}$	49.7 min	555.57	95
^{93}Y	10.17 h	266.9	7.4	^{92}Y	3.54 h	934.47	13.9
$^{95}Zr \rightarrow {}^{95}Nb^{g}$ [b]	64.032 d			$^{95}Zr \rightarrow {}^{95}Nb^{g}$ [b]	64.032 d		
$^{95}Nb^{g}$	34.991 d	765.8	99.81	$^{95}Nb^{g}$	34.991 d	765.8	99.81
^{96}Nb	23.35 h	778.224	96.45	$^{96}Nb^{a}$	23.35 h	460.04	26.62
$^{97}Zr \rightarrow {}^{97}Nb^{g}$ [b]	16.749 h					568.87	58
$^{97}Nb^{g}$	72.1 min	657.94	98.23			1091.35	48.5
$^{98}Nb^{m}$	51.1 min	787.363	13.0			1200.23	19.97
^{99}Mo	65.936 h	140.5	89	$^{97}Zr \rightarrow {}^{97}Nb^{g}$ [b]	16.749 h		
$^{103}Ru^{g}$	39.247 d	497.09	91.0	$^{97}Nb^{g}$	72.1 min	657.94	98.23
^{104}Tc	18.2 min	358	89	$^{99}Mo \rightarrow {}^{99}Tc^{m}$	65.936 h		
^{105}Ru	4.44 h	724.2	47.8	^{99}Mo	65.936 h	140.5 [d]	90.7 [d]
$^{105}Rh^{g}$	35.341 h	319.23	16.9	^{101}Tc	14.02 min	306.83	89
$^{106}Rh^{m}$	131 min	450.8	24.2	$^{103}Ru^{g}$	39.247 d	497.09	91
^{107}Rh	21.7 min	302.77	66	^{105}Ru	4.44 h	724.21	47.8
$^{111}Ag^{g}$	7.421 d	342.13	6.7	$^{105}Rh^{g}$	35.341 h	319.23	16.9
$^{111}Pd^{m}$	5.565 h	172.18	46	$^{106}Rh^{m}$ [a]	131 min	429.4	13.3
^{112}Ag	3.15 h	617.517	43			450.8	24.2
$^{114}In^{m}$	49.51 d	190.27	15.56			717.2	28.9
$^{116}In^{m}$	54.1 min	1293.56	84.8			748.5	19.3
$^{117}Sn^{m}$	13.94 d	158.56	86.4			1046.7	30.4
$^{118}Sb^{m}$	5.01 h	253.678	99	$^{111}Cd^{m}$	48.5 min	245.4	94
$^{119}Te^{m}$	4.69 d	153.59	66	^{112}Ag	3.15 h	617.52	43
$^{120}Sb^{m}$	5.76 d	1023.3	99.4	$^{114}In^{m}$	49.51 d	190.27	15.56
$^{121}Te^{g}$	19.17 d	573.14	80.4	$^{116}In^{m}$ [a]	54.1 min	1097.28	58.5
^{124}I	4.1760 d	602.73	62.9			1293.56	84.8
^{125}Xe	16.962 h	188.418	53.8	$^{117}In^{g}$ [c]	43.2 min	158.6	87
^{126}I	12.93 d	388.633	34.1	$^{117}Sn^{m}$	13.94 d	158.6	86.4
^{127}Xe	36.344 d	202.8	68.7	$^{117}Sb^{c}$	2.80 h	158.56	85.9
^{129}Cs	32.13 h	371.918	30.6	$^{119}Te^{m}$ [a]	4.69 d	153.59	66
$^{131}Ba^{g}$	11.52 d	216.08	20.4			1212.73	66.1
^{132}Cs	6.480 d	667.714	97.59	$^{120}Sb^{m}$ [a]	5.76 d	197.3	87
^{132}La	4.58 h	464.55	76			1171.7	100
$^{133}Ba^{m}$	38.87 h	275.92	17.69	^{129}Cs	32.13 h	411.49	22.3

[a] In the case of multiple interference-free γ-rays, the average value of the yield was used (see text for details)
[b] Yield determined by fitting the parent-daughter decay growth equation to the decay profile of the daughter
[c] Yield determined by solving the equation for mixed activity source considering contributions from more than one radionuclide
[d] Data on γ-ray energy and abundance, based on $^{99}Mo \rightarrow {}^{99}Tc^{m}$ equilibrium, taken from Ref. [49]

Table 2 Formation cross-sections of the fission products measured in the present study in the ^{35}Cl + ^{176}Yb reaction at 167.1 MeV beam energy

S. no.	Nuclide	Type of yield	Cross-section (mb)
1	^{71}Zn^{m}	I	0.29 ± 0.04
2	^{72}Zn	C	0.31 ± 0.11
3	^{72} Ga	I	0.45 ± 0.14
4	^{73} Ga	C	0.87 ± 0.04
5	^{74}As	I	0.31 ± 0.03
6	^{76}As	I	0.77 ± 0.03
7	^{77}Ge	C	0.42 ± 0.04
8	^{82}Br^{g}	I	1.54 ± 0.02
9	^{84}Rb^{g}	I	0.95 ± 0.03
10	^{86}Rb^{g}	I	3.71 ± 0.20
11	^{90}Y^{m}	I	2.29 ± 0.03
12	^{91}Sr	C	2.11 ± 0.14
13	^{91}Y^{m}	I	5.66 ± 0.19
14	^{92}Sr	C	0.80 ± 0.03
15	^{93}Y	C	3.20 ± 0.32
16	^{95}Zr	C	3.86 ± 0.10
17	^{95}Nb^{g}	I	3.36 ± 0.04
18	^{96}Nb	I	4.11 ± 0.03
19	^{97}Zr	C	1.16 ± 0.05
20	^{97}Nb^{g}	I	9.48 ± 0.27
21	^{98}Nb^{m}	I	2.04 ± 0.07
22	^{99}Mo	C	6.57 ± 0.01
23	^{103}Ru^{g}	C	8.24 ± 0.03
24	^{104}Tc	C	1.03 ± 0.14
25	^{105}Ru	C	4.38 ± 0.11
26	^{105}Rh^{g}	C	10.55 ± 0.18
27	^{106}Rh^{m}	I	3.17 ± 0.18
28	^{107}Rh	C	5.19 ± 0.23
29	^{111}Pd^{m}	I	0.84 ± 0.05
30	^{111}Ag^{g}	C	4.73 ± 0.16
31	^{112}Ag	C	5.56 ± 0.17
32	^{114}In^{m}	I	1.69 ± 0.10
33	^{116}In^{m}	I	3.16 ± 0.10
34	^{117}Sn^{m}	I	3.10 ± 0.01
35	^{118}Sb^{m}	I	1.14 ± 0.02
36	^{119}Te^{m}	I	0.23 ± 0.01
37	^{120}Sb^{m}	I	1.72 ± 0.01
38	^{121}Te^{g}	CE	1.40 ± 0.02
39	^{124}I	I	2.38 ± 0.02
40	^{125}Xe	CE	0.68 ± 0.02
41	^{126}I	I	1.90 ± 0.04
42	^{127}Xe	CE	1.17 ± 0.02
43	^{129}Cs	CE	1.02 ± 0.05
44	^{131}Ba^{g}	CE	0.52 ± 0.05
45	^{132}Cs	I	0.64 ± 0.01
46	^{132}La	CE	0.27 ± 0.04
47	^{133}Ba^{m}	I	0.53 ± 0.07

'C' and 'I' stand for the cumulative and independent formation cross-sections of the fission products, respectively. 'CE' represents the cumulative formation cross-section of the fission products having the precursor contribution only from the neutron-deficient side of the β-stability line. The uncertainty in the cross-section is due to the uncertainty associated with the peak area of the characteristic γ-rays. Additional uncertainties could be present due to other sources like efficiency calibration, clock time, decay constant, and γ-ray abundances

attenuation of γ-rays may affect the efficiency calibration, particularly in the case of low-energy γ-rays. Uncertainty due to the other sources, such as clock time, decay constant, and γ-ray abundances would be negligible compared to the above-mentioned sources. An upper limit of the uncertainty from sources other than the peak area was estimated to be around 15%. For the cases where precursor contribution was present, the decay profile of the daughter isotopes was fitted using the parent-daughter decay-growth equation, wherever feasible, depending on the half-lives of parent and daughter with respect to the cooling time. In such cases, the quoted uncertainty on the fission product yields is due to the fitting error.

The measured fission product cross-sections in the ^{35}Cl + ^{176}Yb reaction were normalized using a normalization factor obtained from the ratio of experimental and GEF yields in the symmetric mass region, i.e., 98–106 mass range, for comparison. Similarly, the measured fission product yields for the ^{35}Cl + ^{165}Ho reaction were normalized using the ratio of experimental and GEF yields in the 95–99 mass region. The yields obtained after normalization for both the fissioning systems have been plotted in Fig. 3.

3 Results and discussion

3.1 Calculation of the charge distribution parameters

It has been observed that a large number of fission products identified for both the fissioning systems didn't have contribution in their yields from their precursors in the β-decay chain. These independent yields are represented by hollow triangles in Fig. 3. This is a consequence of the fissioning system being neutron-deficient, resulting in the formation of fission products near the beta stability line. The independent

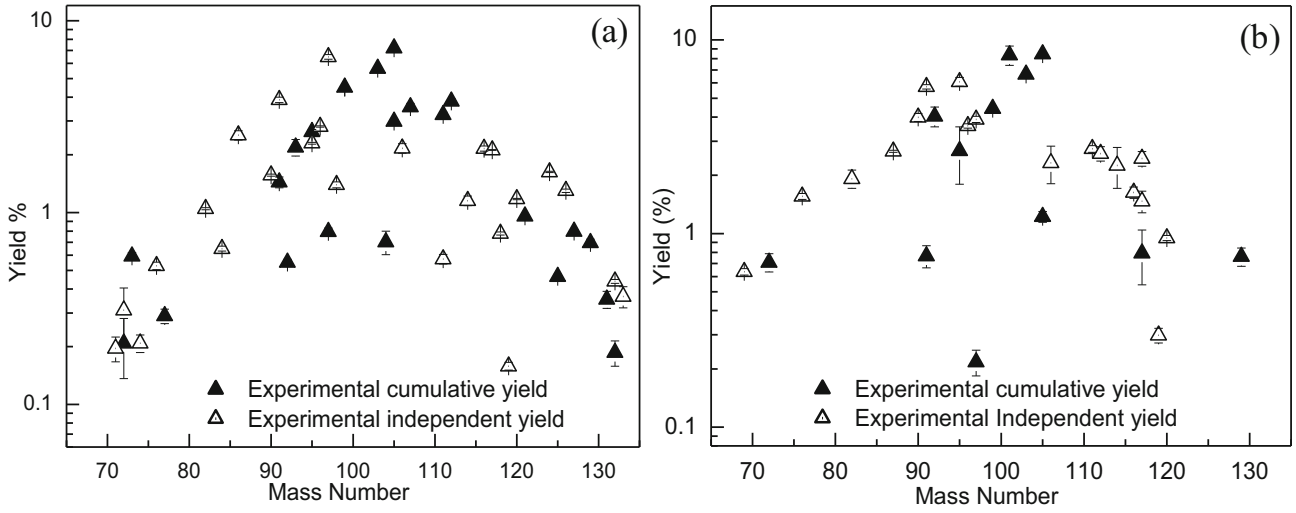

Fig. 3 Measured yields of the identified fission products in the $^{35}Cl + ^{176}Yb$ reaction (**a**) and, $^{35}Cl + ^{165}Ho$ reaction (**b**). Yields have been normalized with respect to GEF values for comparison (see text for details)

yields in a given isobaric chain can be represented by a Gaussian distribution. The experimentally measured cumulative ($CU(A,Z)$) or independent ($IN(A,Z)$) yields should be corrected for the charge distribution to obtain the corresponding mass yields using the following Eqs. (3–6) [45, 51–61]

$$Y(A) = \frac{CU(A,\ Z)}{FC(A,\ Z)} \tag{3}$$

$$Y(A) = \frac{IN(A,\ Z)}{FI(A,\ Z)} \tag{4}$$

$$FC(A,\ Z) = \frac{1}{\sqrt{2\pi\sigma_Z^2}} \int_{-\infty}^{Z+0.5} e^{-(Z-Z_p)^2/2\sigma_Z^2} dZ \tag{5}$$

$$FI(A,\ Z) = \frac{1}{\sqrt{2\pi\sigma_Z^2}} \int_{Z-0.5}^{Z+0.5} e^{-(Z-Z_p)^2/2\sigma_Z^2} dZ \tag{6}$$

where $FC(A,Z)$ and $FI(A,Z)$ are the fractional cumulative and independent yields, respectively. Thus, obtaining the mass yields using the measured fission product yields require the two charge distribution parameters: the most probable charge, Z_P and the width parameter of the isobaric chain, σ_Z. In an ideal case, the knowledge of the independent yields of at least three members of a single isobaric chain is required to calculate the charge distribution parameters, which is usually difficult to obtain experimentally. The most probable charge, Z_P for a mass chain with mass number A, based on the unchanged charge density (UCD) hypothesis, can be given as

$$Z_P = \frac{A}{(A_{cn} - \nu_T)/Z_{cn}} \tag{7}$$

where, A_{cn} and Z_{cn} are the compound nucleus mass and proton numbers, respectively and ν_T is the total number of neutrons evaporated in the fission process. Equations (3–7) can be used to determine the ratio of yields of any two members of the isobaric chain, which would depend on the value of σ_Z and ν_T. As given in Table 1, parent–daughter decay-growth equations were solved by fitting the measured activity of the daughter product at different cooling times. The measured activity of the daughter isotopes for four parent-daughter pairs, i) $^{72}Zn \rightarrow {}^{72}Ga$; ii) $^{91}Sr \rightarrow {}^{91}Y^m$; iii) $^{95}Zr \rightarrow {}^{95}Nb^g$ and iv) $^{97}Zr \rightarrow {}^{97}Nb^g$ was fitted in the case of the $^{35}Cl + ^{176}Yb$ reaction, while the activity for three parent-daughter pairs, i) $^{91}Sr \rightarrow {}^{91}Y^m$; ii) $^{95}Zr \rightarrow {}^{95}Nb^g$ and iii) $^{97}Zr \rightarrow {}^{97}Nb^g$ was fitted in the case of the $^{35}Cl + ^{165}Ho$ reaction. This exercise gives cumulative ($Y_{Z\text{-}1}{}^C$) and independent ($Y_Z{}^I$) yields of the parent and the daughter, respectively. The ratio of the experimentally determined yields $Y_Z{}^I/Y_{Z\text{-}1}{}^C$ was compared with those calculated using the above set of Eqs. (3–7), and best agreement was obtained between the experimental and calculated ratios by varying the value of ν_T and keeping the σ_Z value as a free parameter during the fitting process for both the fissioning systems. The comparison of experimental and calculated values of the ratio $Y_Z{}^I/Y_{Z\text{-}1}{}^C$ is shown in Fig. 4.

As seen from Fig. 4, good agreement has been achieved among experimental and calculated values of the ratio $Y_Z{}^I/Y_{Z\text{-}1}{}^C$ for both the fissioning systems. The corresponding values of ν_T and σ_Z for the $^{35}Cl + ^{176}Yb$ fissioning system were obtained to be 6.7 ± 0.1 and 0.56 ± 0.01, which were found to be in agreement with those obtained using GEF calculations as 6.5 ± 1.1 and 0.63 ± 0.10, respectively. Similarly, the values of ν_T and σ_Z for the $^{35}Cl + ^{165}Ho$ reaction were obtained to be 6.5 ± 0.5 and 0.74 ± 0.01, which

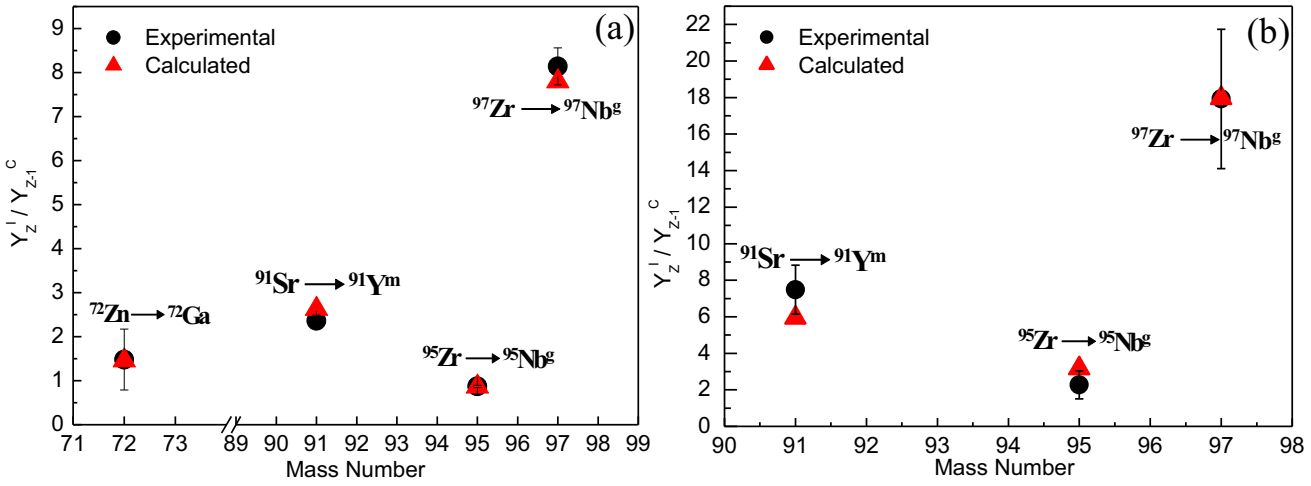

Fig. 4 Experimental and calculated ratios of the independent yield (Y_Z^I) of a member of an isobaric chain and cumulative yield (Y_{Z-1}^C) of its precursor for ^{35}Cl + ^{176}Yb reaction (**a**) and, ^{35}Cl + ^{165}Ho reaction (**b**). Calculated values have been obtained by varying the parameters for charge distribution correction to achieve best agreement with the experimental values (see text for details)

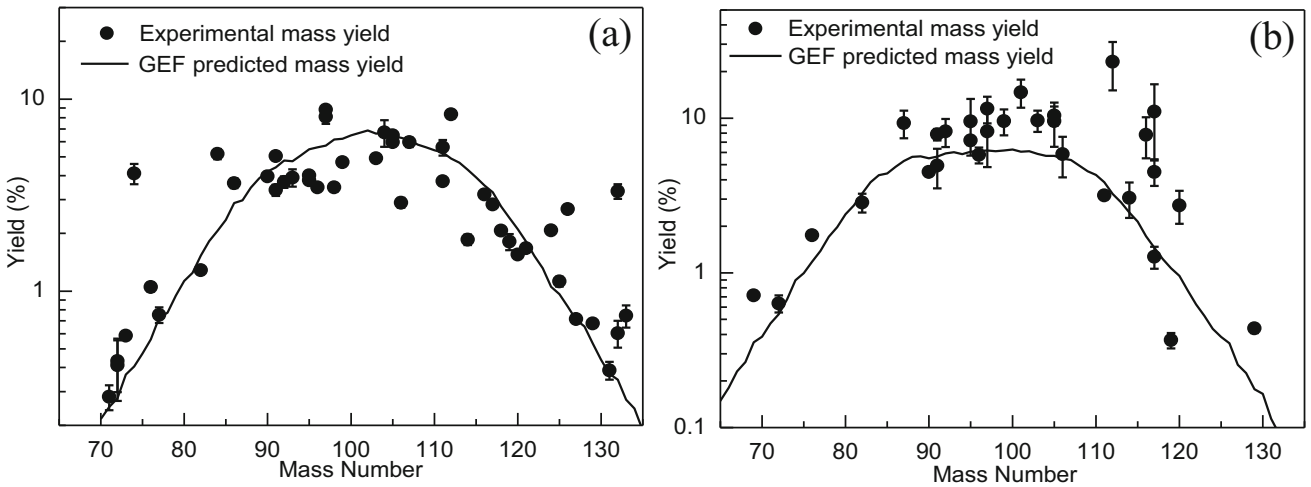

Fig. 5 Normalized mass distributions for the ^{35}Cl + ^{176}Yb reaction at a beam energy of 167.1 MeV (**a**) and, for the ^{35}Cl + ^{165}Ho reaction at a beam energy of 161.7 MeV (**b**), along with the calculations of "GEF, Version 2021/1.1" code (solid line) (see text for details)

were found to agree with the values obtained using GEF calculations as 5.6 ± 1.0 and 0.75 ± 0.07, respectively. The measured fission product yields were converted into the corresponding mass yields using the above-mentioned charge distribution parameters. The experimental mass yields have been normalized by the ratio of the sum of experimental mass yields to the sum of corresponding GEF predicted mass yields. The mass distributions along with the GEF predictions have been plotted for both the fissioning systems in Fig. 5. The uncertainty in the experimental mass yields of the fission products comprises of the uncertainty associated with the measured fission product yields and that with the most probable charge, Z_P, arising from the uncertainty in the ν_T. The effect of uncertainty in the σ_Z was observed to be comparatively negligible. It should be mentioned here that, for fission products having one or more isomers that didn't contribute to the experimentally measured yield, correction was performed using the isomeric yield data obtained from GEF calculations ('GEF', version, 2021/1.1). In the ^{35}Cl + ^{176}Yb reaction, such corrections were less than 10% except in the case of ^{90}Y, ^{121}Te, and ^{132}La for which it was ≈ 16%, ≈ 16%, and ≈ 22%, respectively. Similarly, in the ^{35}Cl + ^{165}Ho reaction, such corrections were less than 10% except in the case of ^{90}Y for which it was ≈ 20%. Further, because of the neutron-deficient light mass fissioning systems, a peculiar situation arises where a few measured fission products have precursor contributions from the neutron-deficient side of the β stability line. In the ^{35}Cl + ^{176}Yb reaction, such products were ^{121}Te^{g}, ^{125}Xe, ^{127}Xe, ^{129}Cs, ^{131}Ba^{g} and ^{132}La, while in the ^{35}Cl + ^{165}Ho reaction, the products having precursor

contribution only from the neutron-deficient side of the β stability line were found to be $^{87}Y^{m}$, ^{117}Sb and ^{129}Cs. For such fission products, the integration limits during the charge distribution correction were accordingly modified to obtain the mass yields.

It can be seen from Fig. 5a that the mass distribution in the $^{35}Cl + ^{176}Yb$ reaction obtained after charge distribution correction shows a broad Gaussian behaviour, indicating a dominant contribution from symmetric fission. However, significant deviation was observed from the symmetric behaviour in the mass region around 124–126, 132–133, and its complementary fission products in the lower mass region around 84–86 and 72–74. The low-energy fission studies by Schmidt et al. [13] proposed a symmetric fission mode contributing to the yields of fission products for the ^{211}Fr fissioning system. However, the charge distribution study of ^{215}Fr at 61 MeV excitation energy by Miernik et al. [14] showed a significant contribution from the asymmetric fission mode (11.6 $\pm$ 2.9%) corresponding to Z $\approx$ 54–56 along with dominant symmetric fission. The GEF (Version 2021/1.1) calculation for the $^{35}Cl + ^{176}Yb$ reaction at 167.1 MeV beam energy, predicts symmetric fission along with approximately 10% contribution from asymmetric component corresponding to Z $\approx$ 38. The GEF predictions were found to be in gross agreement with the experimentally obtained mass distribution for the $^{35}Cl + ^{176}Yb$ reaction.

The nature of the mass distribution obtained in the $^{35}Cl + ^{165}Ho$ reaction at 161.7 MeV (Fig. 5b) couldn't be conclusively established as Gaussian or flat-top nature, mainly due to the large contribution from symmetric fission. As seen from Fig. 5b, the GEF predicted mass distribution (solid line), having $\approx$ 16% contribution from asymmetric component corresponding to Z $\approx$ 38 along with the symmetric component, grossly agrees with the experimental mass distribution in the $^{35}Cl + ^{165}Ho$ reaction. The asymmetric nature of the mass distribution has been observed in the fission of several nuclei in the pre-actinide region, including $^{208,210,212}Po$ at an excitation energy of $\approx$ 10 MeV above the barrier by Itkis et al. [15]. The study in ref. [15] was mainly focused towards investigating the contribution from asymmetric SI and SII modes, discovered earlier in the asymmetric fission observed in the actinide region. Recently, Mahata et al. [12] attributed the asymmetric fission contribution in the pre-actinide region to the proton shell closure around Z $\approx$ 36 of fragments with octupole deformation at scission. Earlier calculations by Wilkins et al. also predicted the deformed proton shells around Z $\approx$ 36 and $\approx$ 38 [7]. Recently, Bogachev et al. [27] measured fission fragment mass and total kinetic energy (TKE) distributions in the fission of $^{180,190}Hg$ and $^{184,192,202}Pb$ using ^{36}Ar and $^{40,48}Ca$ beams in the compound nucleus excitation energy range of 34.1–57.2 MeV. Based on these studies, it was concluded that the three asymmetric fission modes, which are associated with the fragment proton shells corresponding to Z $\approx$ 36, 38; $\approx$ 45, 46 and $\approx$ 28/50, may be present in the mass distribution in the pre-actinide region. The variation in the proton number for a given asymmetric mode, for example, 36 and 38 or 45 and 46, is related to the neutron number of the fragments arising from different fissioning systems. Similarly, in another recent study of the fission fragment mass distribution in the fission of ^{178}Pt and $^{180,182,183}Hg$ in the compound nucleus excitation energy range of 34–71 MeV using ^{36}Ar and ^{40}Ca beams, proton shells corresponding to Z $\approx$ 36 and $\approx$ 46 have been proposed to be responsible for the contribution from asymmetric components [28]. The charge distribution studies of fission fragments in the sub-lead region by Morfouace et al. [32] highlighted the role of deformed proton shell of the light fragment at Z = 36. The fission fragment mass distributions studies for $^{176,186}Pt$ studied at various excitation energies by Duan et al. [33] proposed the dominant role of the proton shells corresponding to $Z \approx 35$ for the light fragments and $Z \approx 43$ for the heavy fragments. Similarly, heavy-ion induced fission mass distributions studies by Buete et al. [34] attributed the proton shell gaps at Z = 34,36 and Z = 44,46 to be major guide for the fission mass distributions in the sub-lead and the pre-actinide region. Thus, the mass distribution observed in the present study by γ-ray spectrometry of fission products formed in the $^{35}Cl + ^{165}Ho \rightarrow ^{200}Po$ reaction is in line with the recent studies on the mass distribution in the pre-actinide region.

As seen from Fig. 5, though, the nature of the experimental mass distribution is in gross agreement with the GEF calculations, some of the experimental mass yields show large deviation from the GEF calculations without any specific trend. This may be a consequence of several factors, like the deviation of Z_P values from those estimated based on the UCD hypothesis (Z_{UCD}) due to the charge polarization [62], secondary de-excitation, or due to shell effects in addition to those considered by the GEF. In a recent study by Schmitt et al. [26], measurement of the average neutron to proton ratio $<N>/Z$ of the fission fragments in the fission of ^{178}Hg showed a strong charge polarization effect resulting in a significant deviation of measured $<N>/Z$ values from those based on the UCD hypothesis. The deviation of $<N>/Z$ values, if translated into Z_P values, would become more than $\approx$2 units for the masses at the extreme ends of the mass distribution. To identify the mass yields with deviations beyond the possible variation caused by charge distribution correction, Z_P values were varied in the range of $\pm$ 1.5 units from Z_{UCD} while obtaining the corresponding mass yields. The variation in Z_P within $\pm$ 1.5 units from those estimated using the UCD hypothesis was done to achieve the best agreement between the experimental and GEF calculated mass yields. Comparison of GEF normalized experimental mass yields with those obtained with the GEF calculations for both the fissioning systems has been shown in Fig. 6a, b, and the corresponding

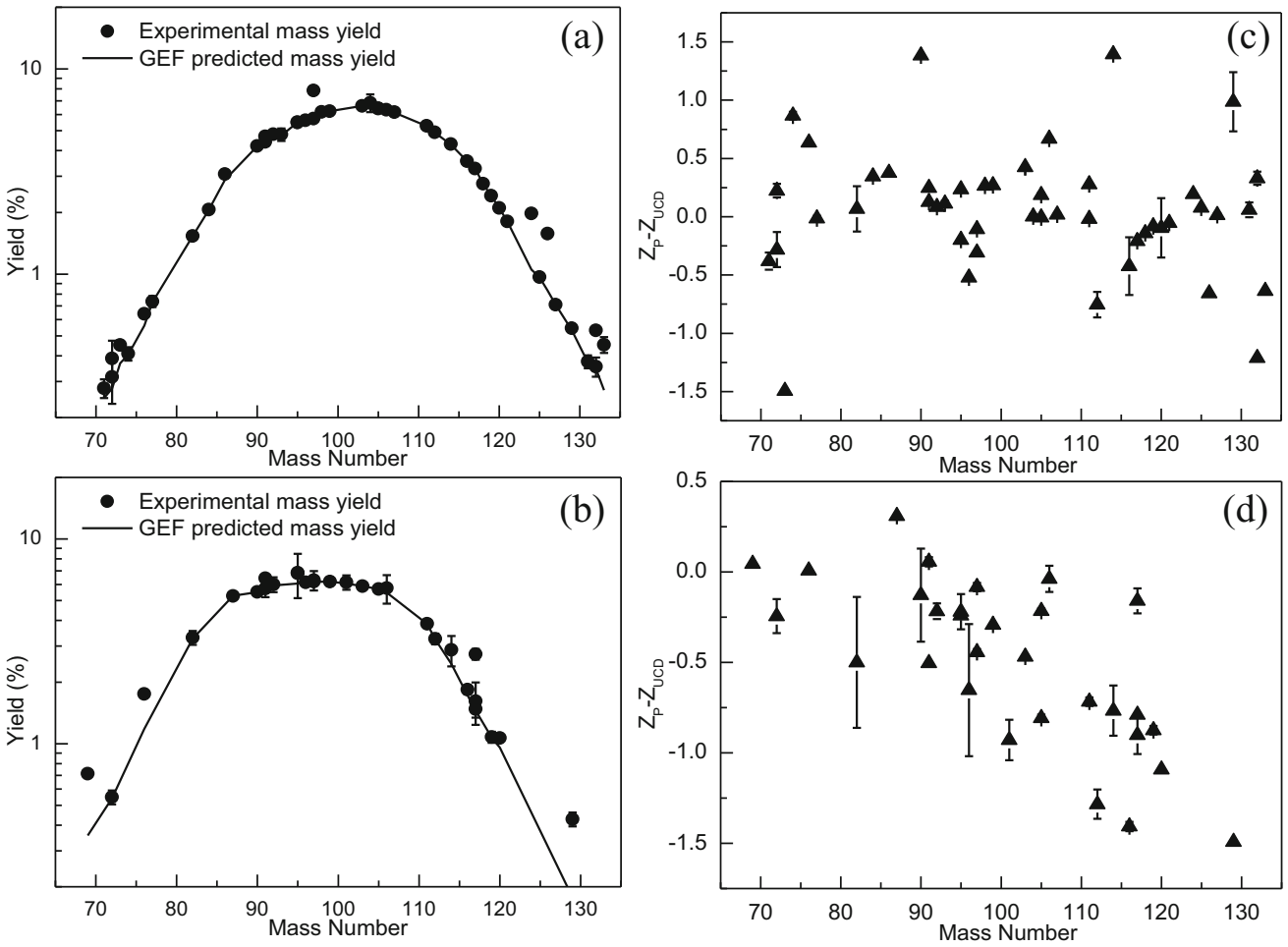

Fig. 6 Normalized mass yield distributions for ^{35}Cl + ^{176}Yb reaction at the beam energy of 167.1 MeV (**a**) and, ^{35}Cl + ^{165}Ho reaction at the beam energy of 161.7 MeV (**b**), after allowing the variation of Z_P values obtained using UCD hypothesis within ± 1.5 unit to achieve best possible agreement between experimental and "GEF, Version 2021/1.1" predicted mass yields. The corresponding plot of (Z_P-Z_{UCD}) versus the mass number for ^{35}Cl + ^{176}Yb (**c**) and, ^{35}Cl + ^{165}Ho (**d**) reactions

values of Z_P-Z_{UCD} has been shown as a function of mass number in Fig. 6c, d.

For some of the independent fission product yields in the ^{35}Cl + ^{165}Ho reaction, two Z_P values could match the GEF calculated mass yields. In such cases, Z_P values giving positive (negative) deviations for the fission products having mass below (above) the symmetric mass i.e., 97 were considered. It can be seen from Fig. 6 that the best agreement between the experimental and the calculated mass yields can be achieved for most of the masses by varying the Z_P values with respect to the Z_{UCD} values. These variations can be considered reasonable as they are within the limits expected based on the charge polarization effect observed by Schmitt et al. [26]. In addition to the charge polarization, the secondary de-excitation effect would also be present. There was no specific trend observed for the deviation of the Z_P values from Z_{UCD} in the ^{35}Cl + ^{176}Yb reaction. However, the direction of the deviation of the Z_P values from Z_{UCD} in the ^{35}Cl + ^{165}Ho reaction was found to be the same as observed in the actinide region. This observation suggests that the fission products formed in the present study are not sufficiently neutron-deficient to reverse the direction of the deviation as observed by Schmitt et al. [26] for the compound nucleus ^{178}Hg. As seen from Fig. 6, some experimental mass yields still deviate from the GEF calculations for both the fissioning systems. It is interesting to note that the deviations are observed only in the positive direction. In order to observe the magnitude of these deviations, the ratio of GEF normalized experimental to the GEF calculated mass yields has been plotted in Fig. 7a, b as a function of mass number. The ratio of the normalized experimental to GEF calculated fission product yields for the corresponding masses showing deviations from GEF has been plotted in Fig. 7c, d. It can be seen from Fig. 7a, b that, for some of the fission products, these

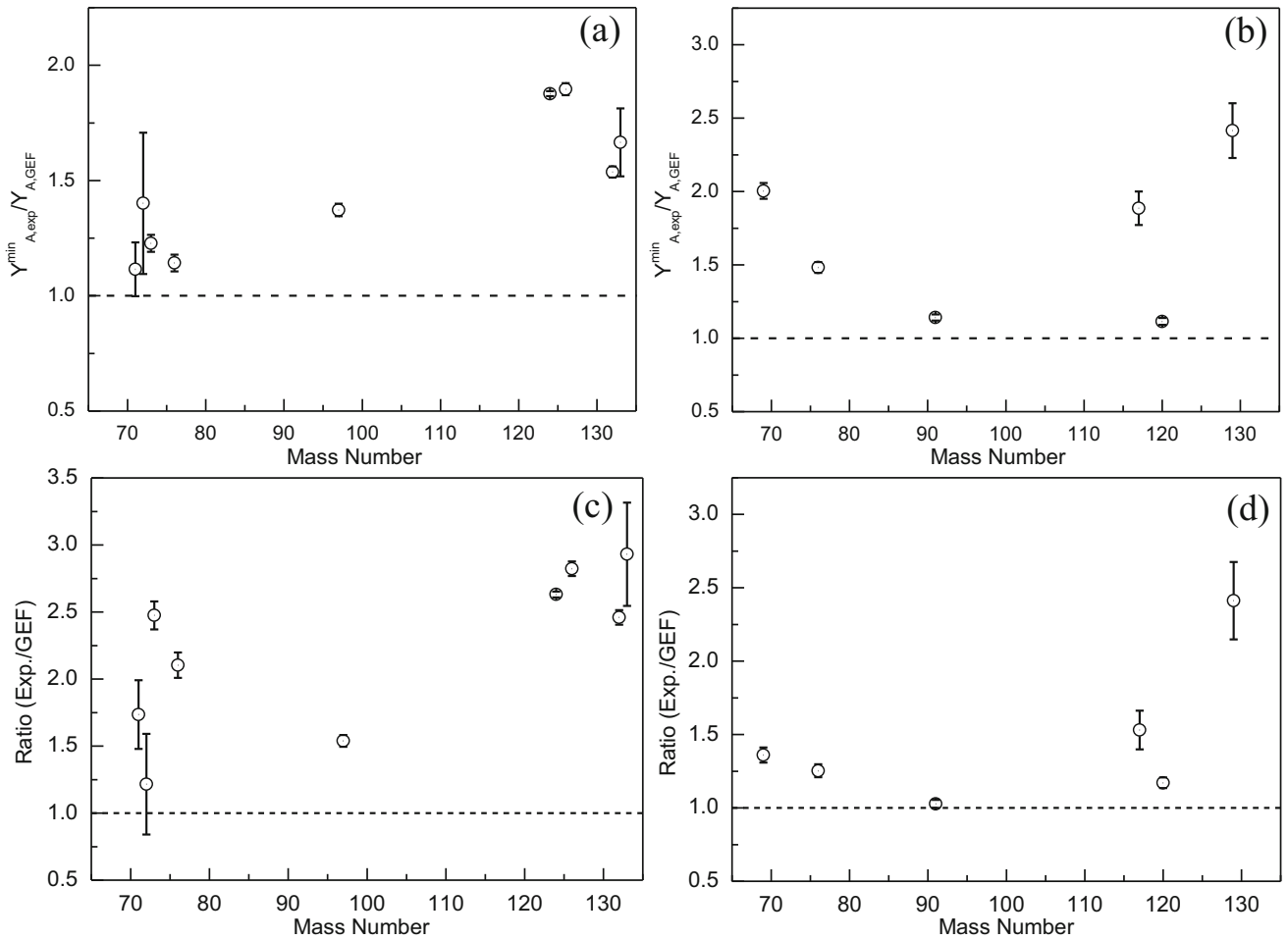

Fig. 7 Plot of the ratio of GEF Normalized experimental mass yields to GEF calculated mass yields for the ^{35}Cl + ^{176}Yb reaction (**a**) and, the ^{35}Cl + ^{165}Ho reaction (**b**) for the mass chains for which agreement between experimental and calculated values could not be achieved even after allowing the variation in the Z_P values based on UCD hypothesis. Plot of the ratio of GEF Normalized experimental fission product yields to GEF calculated fission product yields for ^{35}Cl + ^{176}Yb reaction (**c**) and, ^{35}Cl + ^{165}Ho reaction (**d**)

deviations are more than 50% and cannot be attributed to any possible uncertainty arising from experimental measurements or theoretical calculations. Such products are ^{72}Zn, ^{124}I, ^{126}I, ^{132}Cs, and ^{133}Ba in case of the ^{35}Cl + ^{176}Yb reaction, whereas, in the ^{35}Cl + ^{165}Ho reaction, ^{69}Zn, ^{117}Sn, and ^{129}Cs were found to have the deviations greater than 50% from the GEF predicted values. It can be seen from Fig. 7c, d that the fission products that exhibited deviations in mass yields also showed deviations from the GEF calculations in their product yields.

It should be mentioned here that these deviations correspond to mass yields which were obtained with minimum charge distribution correction to the experimental yields. For independent yields, this would be a natural consequence of the Z_P variation procedure, which would make the Z_P value coincide with the Z of the measured fission product to keep the charge distribution correction minimum (see Eq. 6). This approach applies particularly to yields that are unusually high and cannot be matched with the theoretical value under any condition. Thus, actual deviation may be even higher and the deviations shown in Fig. 6 should be considered as lower limits. The large deviations of these data points from GEF calculations need to be explained. Any modification of the isobaric yield distributions corresponding to different mass chains due to the possible presence of quasifission causes change in the charge distribution correction parameters. Such changes would increase the correction factor and, consequently, further increase the deviations. It should be mentioned here that fragment shell effects near scission can be present in the case of quasifission also, or even may be driven by quasifission [63, 64]. Thus, the charge distribution correction procedure provides an opportunity to look into the role of specific nucleon shells irrespective of the presence or absence of quasifission. The observed deviations may be due

to the presence of shell effects in addition to those considered in the GEF calculations or the secondary de-excitation effects. The GEF considers the contribution from the asymmetric fission mode corresponding to Z ≈ 38, along with symmetric fission in this mass region. However as observed in the present studies, the large deviations in the higher mass region correspond to the measured yields of fission products ^{124}I, ^{126}I (Z = 53) and ^{132}Cs (Z = 55), ^{133}Ba (Z = 56) in the ^{35}Cl + ^{176}Yb reaction and, ^{117}Sn (Z = 50) and ^{129}Cs (Z = 55) in the ^{35}Cl + ^{165}Ho reaction along with similar deviations in the complementary lighter mass region. The present observations indicate the possible role of conventional SI (corresponding to Z ≈ 50–52) and SII (corresponding to Z ≈ 54–56) modes as observed in the actinide region [31]. This is consistent with the observation of the presence of SI and SII modes by Itkis et al. in similar fissioning systems [15]. A similar observation of the presence of an asymmetric fission mode corresponding to Z ≈ 54–56 along with the dominant symmetric fission for ^{215}Fr at a similar excitation energy was reported by Miernik et al. [14]. The heavy-ion induced fission mass distributions studies for the even-Z fissioning nuclei by Buete et al. [34] didn't rule out the contribution from the proton shells associated with asymmetric SI and SII fission modes. Further studies involving the measurement of more yields of charge and mass identified fission products/fragments around Z ≈ 50–52 and Z ≈ 55–56 are required to confirm the contribution from specific asymmetric fission modes operating in the pre-actinide region. The asymmetric components would mainly arise from the higher chance fission. Based on the GEF calculations, 4th and 5th chance fission together constitute 38.0% and 34.3% of the total fission in the ^{35}Cl + ^{176}Yb and the ^{35}Cl + ^{165}Ho reactions, respectively. It is important to note that the proton numbers corresponding to SI and SII modes remain nearly constant over a large change in the mass of the fissioning system from the actinide region to the pre-actinide mass region ≈ 200, though mass numbers change significantly.

The overall fission cross-section at a beam energy of 167.1 MeV for the ^{35}Cl + ^{176}Yb reaction was obtained by a 4th order polynomial fitting of the experimental mass distribution and was found to be 185 ± 12 mb. The overall fission cross-section includes the correction due to loss of fission products through the 5 mm diameter hole in the cone on which the backward catcher foil is mounted. The uncertainty quoted on the overall fission cross-section was obtained by fitting the lower and upper limits of the measured yields obtained using the uncertainty on the individual mass yields. The overall fusion cross-section for the ^{35}Cl + ^{176}Yb reaction calculated using the code CCFUS [46] was obtained to be 188 mb. However, in the neutron-deficient light mass fissioning systems, there could be a significant contribution present from the evaporation residues along with the fission events. The fission percentage was calculated using the code PACE4 (Version 4.2) [65–67], which was found to be 87.1% for the ^{35}Cl + ^{176}Yb reaction at 167.1 MeV beam energy. Therefore, the calculated fission cross-section for the ^{35}Cl + ^{176}Yb reaction was found to be 164 mb, which was found to be close to the experimental value.

4 Conclusions

Mass distributions were measured for the ^{35}Cl + ^{176}Yb and ^{35}Cl + ^{165}Ho reactions at 167.1 and 161.7 MeV, respectively, using the recoil catcher technique followed by off-line γ-ray spectrometry. The yields of 47 and 30 fission products were measured for the ^{35}Cl + ^{176}Yb and the ^{35}Cl + ^{165}Ho reactions, respectively, which were converted into the corresponding mass yields using the respective charge distribution parameters. A broad Gaussian mass distribution was observed for the ^{35}Cl + ^{176}Yb reaction, which indicates a dominant contribution from the symmetric fission mode. However, the nature of the mass distribution obtained in the ^{35}Cl + ^{165}Ho reaction at 161.7 MeV couldn't be conclusively established as Gaussian or flat-top nature, mainly due to the large contribution from symmetric fission. The mass distributions obtained in both the fissioning systems were found to be in reasonable agreement with the GEF calculations predicting the contribution from the $Z \approx 38$ asymmetric component. Some of the fission products showed large deviations from the GEF calculations without any specific trend. These deviations could be minimized by allowing variation in the charge distribution parameter Z_P (most probable charge for an isobaric chain) in the range of ± 1.5 units compared to the values obtained using the unchanged charge density (UCD) hypothesis. Strong positive deviations from the GEF calculations were still observed in the mass region 124–126 and 132–133, and in the complementary lower mass region around 84–86 and 72–74, respectively, indicating the contribution from asymmetric fission modes. These deviations indicated the additional shell effects beyond that considered in GEF at $Z \approx 38$. Incidentally, the large deviations observed in the higher mass region correspond to Z ≈ 50–52 and Z ≈ 54–56, along with similar deviations in the lighter mass region which correspond to the conventional asymmetric modes SI and SII observed in the actinide region. Further studies in nearby systems would help to confirm these observations.

Acknowledgements The authors thank the operating staff of the BARC-TIFR Pelletron-LINAC facility for providing the ^{35}Cl beam. The authors also thank Prof. V. Nanal for providing help during the experiment.

Funding Open access funding provided by Department of Atomic Energy.

Data availability Data will be made available on reasonable request. [Author's comment: The datasets generated during and/or analysed during the current study are available from the corresponding author on reasonable request.]

Code availability Code/software will be made available on reasonable request. [Author's comment: The code/software generated during and/or analysed during the current study is available from the corresponding author on reasonable request.]

Declarations

Conflict of interest The authors declare they have no financial interests.

References

1. K.-H. Schmidt, B. Jurado, C. Amouroux, C. Schmitt, Nucl. Data Sheets **131**, 107 (2016)
2. K.-H. Schmidt, B. Jurado, Rep. Prog. Phys. **81**, 106301 (2018)
3. A.N. Andreyev, J. Elseviers, M. Huyse, P. Van Duppen, S. Antalic, A. Barzakh, N. Bree, T.E. Cocolios, V.F. Comas, J. Diriken, D. Fedorov, V. Fedosseev, S. Franchoo, J.A. Heredia, O. Ivanov, U. Köster, B.A. Marsh, K. Nishio, R.D. Page, N. Patronis et al., Phys. Rev. Lett. **105**, 252502 (2010)
4. T. Ichikawa, P. Moller, Phys. Lett. B **789**, 679 (2019)
5. T. Ichikawa, A. Iwamoto, P. Moller, A.J. Sierk, Phys. Rev. C **86**, 024610 (2012)
6. P. Moller, J. Randrup, A.J. Sierk, Phys. Rev. C **85**, 024306 (2012)
7. B.D. Wilkins, E.P. Steinberg, R.R. Chasman, Phys. Rev. C **14**, 1832 (1976)
8. A.V. Andreev, G.G. Adamian, N.V. Antonenko, Phys. Rev. C **86**, 044315 (2012)
9. A.V. Andreev, G.G. Adamian, N.V. Antonenko, S.P. Ivanova, W. Scheid, Eur. Phys. J. A **22**, 51 (2004)
10. A.V. Andreev, G.G. Adamian, N.V. Antonenko, Phys. Rev. C **93**, 034620 (2016)
11. G. Scamps, C. Simenel, Phys. Rev. C **100**, 041602(R) (2019)
12. K. Mahata, C. Schmitt, S. Gupta, A. Shrivastava, G. Scamps, K.H. Schmidt, Phys. Lett. B **825**, 136859 (2022)
13. K.-H. Schmidt, S. Steinhäuser, C. Böckstiegel, A. Grewe, A. Heinz, A.R. Junghans, J. Benlliure, H.-G. Clerc, M. Jong, J. Müller, M. Pfützner, B. Voss, Nucl. Phys. A **665**, 221 (2000)
14. K. Miernik, A. Korgul, W. Poklepa, J.N. Wilson, G. Charles, S. Czajkowski, P. Czyz, A. Fijałkowska, L.M. Fraile, P. Garczynski, K. Hauschild, C. Hiver, T. Kurtukian-Nieto, M. Lebois, M. Llanos, A. Lopez-Martens, K.M. Deby Treasa, J. Ljungvall, I. Matea, J. Mielczarek, J.R. Murias, G. Pasqualato, A. Skruch, K. Solak, K. Stoyachev, I. Tsekhanovich, Phys. Rev. C **108**, 054608 (2023)
15. M.G. Itkis, V.N. Okolovich, A.Y. Rusanov, G.N. Smirenkin, Z. Phys. A **320**, 434 (1985)
16. L. Ghys et al., Phys. Rev. C **90**, 041301(R) (2014)
17. R. Tripathi, S. Sodaye, K. Sudarshan, B.K. Nayak, A. Jhingan, P.K. Pujari, K. Mahata, S. Santra, A. Saxena, E.T. Mirgule, R.G. Thomas, Phys. Rev. C **92**, 024610 (2015)
18. I. Tsekhanovich, A.N. Andreyev, K. Nishio, D. Denis-Petit, K. Hirose, H. Makii, Z. Matheson, K. Morimoto, K. Morita, W. Nazarewicz, R. Orlandi, J. Sadhukhan, T. Tanaka, M. Vermeulen, M. Warda, Phys. Lett. B **790**, 583 (2019)
19. K. Nishio, A.N. Andreyev, R. Chapman, X. Derkx, C.E. Düllmann, L. Ghys, F.P. Heßberger, K. Hirose, H. Ikezoe, J. Khuyagbaatar, B. Kindler, B. Lommel, H. Makii, I. Nishinaka, T. Ohtsuki, S.D. Pain, R. Sagaidak, I. Tsekhanovich, M. Venhart, Y. Wakabayashi, S. Yan, Phys. Lett. B **748**, 89 (2015)
20. E. Prasad, D.J. Hinde, K. Ramachandran, E. Williams, M. Dasgupta, I.P. Carter, K.J. Cook, D.Y. Jeung, D.H. Luong, S. McNeil, C.S. Palshetkar, D.C. Rafferty, C. Simenel, A. Wakhle, J. Khuyagbaatar, C.E. Düllmann, B. Lommel, B. Kindler, Phys. Rev. C **91**, 064605 (2015)
21. A. Sen, T.K. Ghosh, S. Bhattacharya, K. Banerjee, C. Bhattacharya, S. Kundu, G. Mukherjee, A. Asgar, A. Dey, A. Dhal, M.M. Shaikh, J.K. Meena, S. Manna, R. Pandey, T.K. Rana, P. Roy, T. Roy, V. Srivastava, P. Bhattacharya, Phys. Rev. C **96**, 064609 (2017)
22. S. Gupta, C. Schmitt, K. Mahata, A. Shrivastava, P. Sugathan, A. Jhingan, K.S. Golda, N. Saneesh, M. Kumar, G. Kaur, L. Stuttgé, D. Arora, H. Arora, A. Chatterjee, K. Chauhan, S.K. Duggi, D.P. Kaur, V. Mishra, P.N. Patil, K. Rani, Phys. Rev. C **100**, 064608 (2019)
23. T.N. Nag, R. Tripathi, S. Patra, A. Mhatre, S. Santra, P.C. Rout, A. Kundu, D. Chattopadhyay, A. Pal, P.K. Pujari, Phys. Rev. C **103**, 034612 (2021)
24. S. Gupta, K. Mahata, A. Shrivastava, K. Ramachandran, S.K. Pandit, P.C. Rout, V.V. Parkar, R. Tripathi, A. Kumar, B.K. Nayak, E.T. Mirgule, A. Saxena, S. Kailas, A. Jhingan, A.K. Nasirov, G.A. Yuldasheva, P.N. Nadtochy, C. Schmitt, Phys. Lett. B **803**, 135297 (2020)
25. E. Prasad, D.J. Hinde, M. Dasgupta, D.Y. Jeung, A.C. Berriman, B.M.A. Swinton-Bland, C. Simenel, E.C. Simpson, R. Bernard, E. Williams, K.J. Cook, D.C. Rafferty, C. Sengupta, J.F. Smith, K. Vo-Phuoc, J. Walshe, Phys. Lett. B **811**, 135941 (2020)
26. C. Schmitt, A. Lemasson, K.-H. Schmidt, A. Jhingan, S. Biswas, Y.H. Kim, D. Ramos, A.N. Andreyev, D. Curien, M. Ciemala, E. Clément, O. Dorvaux, B. De Canditiis, F. Didierjean, G. Duchêne, J. Dudouet, J. Frankland, B. Jacquot, C. Raison, D. Ralet, B.-M. Retailleau, L. Stuttgé, I. Tsekhanovich, Phys. Rev. Lett. **126**, 132502 (2021)
27. A.A. Bogachev, E.M. Kozulin, G.N. Knyazheva, I.M. Itkis, M.G. Itkis, K.V. Novikov, D. Kumar, T. Banerjee, I.N. Diatlov, M. Cheralu, V.V. Kirakosyan, Y.S. Mukhamejanov, A.N. Pan, I.V. Pchelintsev, R.S. Tikhomirov, I.V. Vorobiev, M. Maiti, R. Prajapat, R. Kumar, G. Sarkar, W.H. Trzaska, A.N. Andreyev, I.M. Harca, E. Vardaci, Phys. Rev. C **104**, 024623 (2021)
28. E.M. Kozulin, G.N. Knyazheva, I.M. Itkis, M.G. Itkis, Y.S. Mukhamejanov, A.A. Bogachev, K.V. Novikov, V.V. Kirakosyan, D. Kumar, T. Banerjee, M. Cheralu, M. Maiti, R. Prajapat, R. Kumar, G. Sarkar, W.H. Trzaska, A.N. Andreyev, I.M. Harca, A. Mitu, E. Vardaci, Phys. Rev. C **105**, 014607 (2022)
29. A. Jhingan et al., Phys. Rev. C **106**, 044607 (2022)
30. R. Kumar, M. Maiti, A. Pal, S. Santra, P. Kaur, M. Sagwal, A. Singh, P.C. Rout, A. Baishya, R. Gandhi, T. Santhosh, Phys. Rev. C **107**, 034614 (2023)
31. U. Brosa, S. Grossmann, M. Andreas, Phys. Rep. **197**, 167 (1990)
32. P. Morfouace et al., Nature **641**, 339–344 (2025)
33. H.R. Duan, H.M. Jia, C.J. Lin, D.J. Hinde, K. Banerjee, J. Buete, I.P. Carter, K.J. Cook, M. Dasgupta, C. Sengupta, B.M.A. Swinton-Bland, E. Williams, D.X. Wang, F.C. Gu, L. Yang, N.R. Ma, P.W.

Wen, F. Yang, T.P. Luo, H.Q. Zhang, Phys. Rev. C **111**, 044613 (2025)
34. J. Buete, B.M.A. Swinton-Bland, D.J. Hinde, K.J. Cook, M. Dasgupta, A.C. Berriman, D.Y. Jeung, K. Banerjee, L.T. Bezzina, I.P. Carter, C. Sengupta, C. Simenel, E.C. Simpson, Phys. Lett. B **865**, 139459 (2025)
35. R. Vandenbosch, J.R. Huizenga, *Nuclear Fission* (Academic Press, New York, 1973)
36. L.S. Danu, D.C. Biswas, A. Saxena, A. Shrivastava, A. Chatterjee, B.K. Nayak, R.G. Thomas, R.K. Choudhury, R. Palit, I. Mazumdar, P. Datta, S. Chattopadhyay, S. Pal, S. Bhattacharya, S. Muralithar, K.S. Golda, R.K. Bhowmik, J.J. Das, R.P. Singh, N. Madhavan, J. Gerl, S.K. Patra, L. Satpathy, Phys. Rev. C **81**, 014311 (2010)
37. A. Dey, D.C. Biswas, A. Chakraborty, S. Mukhopadhyay, A.K. Mondal, K. Mandal, B. Mukherjee, R. Chakrabarti, B.N. Joshi, L.A. Kinage, S. Chatterjee, S. Samanta, S. Das, S. Bhattacharya, R. Banik, S. Nandi, S. Dar, R. Raut, G. Mukherjee, S. Bhattacharyya, S.S. Ghugre, A. Goswami, Phys. Lett. B **825**, 136848 (2022)
38. S. Kumar, S. Patra, A. Mhatre, A. Kumar, K. Ramachandran, R. Tripathi, Eur. Phys. J. A **60**, 146 (2024)
39. S. Kim, C.J. Martoff, M. Dion, D. Glasgow, Nucl. Instrum. Methods Phys. Res. Sect. A Accel. Spectrom. Detect. Assoc. Equip. **1059**, 169001 (2024)
40. A.P. Tonchev, R.C. Malone, A.P.D. Ramirez, J.A. Silano, M.A. Stoyer, M.E. Gooden, T.A. Bredeweg, J.B. Wilhelmy, S.W. Finch, C.R. Howell, W. Tornow, No. LLNL-PROC-855034. Lawrence Livermore National Laboratory (LLNL), Livermore, CA (United States) (2023)
41. P.D. Ramirez, J.A. Silano, R.C. Malone, M.A. Stoyer, A.P. Tonchev, M.E. Gooden, J.B. Wilhelmy, S.W. Finch, C.R. Howell, Krishichayan, W. Tornow, Phys. Rev. C **107(5)**, 054608 (2023)
42. X. Yang, C. Lan, Y. Nie, L. Jiang, Y. Qiu, Y. Ge, H. Chen, K. Zhang, Y. Wei, J. Wang, G. Jiang, Chin. Phys. C **47**(2), 024001 (2023)
43. Y. Ge, C. Lan, H. Lv, X. Yang, Y. Wei, F. Lu, J. Wang, G. Jiang, B. Li, Y. Yang, X. Ruan, Appl. Radiat. Isot. **200**, 110907 (2023)
44. M. Tohamy, J.M. Crochemore, K. Abbas, S. Nonneman, Nucl. Instrum. Methods Phys. Res. Sect. A Accel. Spectrom. Detect. Assoc. Equip. **978**, 164347 (2020)
45. R. Tripathi, K. Sudarshan, S. Sodaye, B.S. Tomar, G.K. Gubbi, A. Goswami, A.V.R. Reddy, S.B. Manohar, Radiochim. Acta **90**, 185 (2002)
46. C.H. Dasso, S. Landowne, Comput. Phys. Commun. **46**, 187 (1987)
47. National Nuclear Data Center, Brookhaven National Laboratory, NuDat (Nuclear Structure and Decay Data) (2008). https://www.nndc.bnl.gov/nudat3/
48. A.A. Sonzogni, AIP Conf. Proc. **769**, 574 (2005). https://www.nndc.bnl.gov/nudat3/nudat2/
49. U. Reus, W. Westmeier, At. Data Nucl. Data Tables **29**, 1 (1983)
50. P.K. Mukhopadhyaya, in *Proceedings of DAE Symposium on Intelligent Nuclear Instrumentation (INIT-2001)*, ed. by S.K. Kataria, P.P. Vaidya, P.V. Narurkar, S. Roy (BARC, Mumbai, India, 2001), p. 307
51. A.C. Wahl, R.L. Ferguson, D.R. Nethaway, D.E. Troutner, K. Wolfsberg, Phys. Rev. **126**, 1112 (1962)
52. A.C. Wahl, in *Proceedings of the Conference on 50 Years with Nuclear Fission*, vol II (American Nuclear Society, Gaithersburg, 1989), p. 525
53. A. Srivastava, H.O. Denschlag, Radiochim. Acta **46**, 17 (1989)
54. D. De Frenne, H. Thierens, B. Proot, E. Jacobs, P. De Gelder, A. De Clercq, W. Westmeier, Phys. Rev. C **26**, 1356 (1982)
55. B.L. Tracy, J. Chaumont, R. Klapisch, J.M. Nitschke, A.M. Poskanzer, E. Roeckle, C. Thibault, Phys. Rev. C **5**, 222 (1972)
56. J.A. McHugh, M.C. Michel, Phys. Rev. **172**, 1160 (1968)
57. H.M. Blann, Phys. Rev. C **123**, 1356 (1961)
58. W. Reisdorf, M. de Saint-Simon, L. Remsberg, L. Lessard, C. Thibault, E. Roeckl, R. Klapisch, Phys. Rev. C **14**, 2189 (1976)
59. G.K. Gubbi, A. Goswami, B.S. Tomar, B. John, A. Ramaswami, A.V.R. Reddy, P.P. Burte, S.B. Manohar, Phys. Rev. C **53**, 796 (1996)
60. R. Tripathi, K. Sudarshan, A. Goswami, P.K. Pujari, B.S. Tomar, S.B. Manohar, Phys. Rev. C **69**, 024613 (2004)
61. R. Tripathi, K. Sudarshan, A. Goswami, R. Guin, A.V.R. Reddy, Phys. Rev. C **74**, 014610 (2006)
62. H. Kudo, M. Maruyama, M. Tanikawa, Phys. Rev. C **57**, 178 (1998)
63. A.Yu. Chizhov, M.G. Itkis, I.M. Itkis, G.N. Kniajeva, E.M. Kozulin, N.A. Kondratiev, I.V. Pokrovsky, R.N. Sagaidak, V.M. Voskressensky, A.V. Yeremin, L. Corradi, A. Gadea, A. Latina, A.M. Stefanini, S. Szilner, M. Trotta, A.M. Vinodkumar, S. Beghini, G. Montagnoli, F. Scarlassara, A.Y. Rusanov, F. Hanappe, O. Dorvaux, N. Rowley, L. Stuttgé, Phys. Rev. C **67**, 011603(R) (2003)
64. A. Pal, S. Santra, P.C. Rout, A. Kundu, D. Chattopadhyay, R. Gandhi, P.N. Patil, R. Tripathi, B.J. Roy, Y. Sawant, T.N. Nag, A. Baishya, T. Santhosh, P.K. Rath, N. Deshmukh, Phys. Rev. C **110**, 034601 (2024)
65. O.B. Tarasov, D. Bazin, Nucl. Instrum. Methods Phys. Res. Sect. B Beam Interact. Mater. Atoms **266**, 4657–4664 (2008)
66. A. Gavron, Phys. Rev. C **21**, 230–236 (1980)
67. http://lise.nscl.msu.edu/pace4